



Synthesis of polyamide-6: Characterization and application to the removal of heavy metals by clays

Zoulikha Khiati¹ & Lahouari Mrah^{*2,3}

¹Département de chimie-physique, Faculté de chimie, Université des Sciences et de la Technologie d'Oran, M. Boudiaf, BP 1505 El M'naouar, 31000 Oran, Algeria

²Laboratoire de Chimie des Polymères (LCP), Faculté des sciences exactes et appliquées, Université Oran1 Ahmed Ben Bella, BP 1524, El Mnaouar 31000, Oran, Algérie

³Ecole supérieure en génie électrique et énergétique d'Oran, ESGEE, Chemin Vicinal N9, Oran, 31000, Algérie

E mail : lmrah@yahoo.fr

Received 3 April 2022; accepted 17 June 2022

Using maghnite as an inorganic reinforcement, polyamide-6-based nanocomposites (PA6/Mag-CTA) have been synthesized. Maghnite is a type of laminar clay, which is distinguished by a significantly higher $\text{SiO}_2/\text{Al}_2\text{O}_3$ ratio than other clays in the world. It is likely that the interfacial cations of maghnite form active sites during the reaction, and thus give it a catalytic behaviour. This work focuses on the preparation and characterization of polyamide-6/organic clay nanocomposites. The effect of the nature of organo-modified clay, and the preparation method have been studied to assess their structural, morphological and thermal properties, as well as their mechanical properties. Diverses compositions de PA6-Mag-CTA ont été élaborées en intégrant 1, 3, 5 et 7% de Mag-CTA. The formation of polyamide-6 has been confirmed by X-ray diffraction (XRD), spectroscopy (IR), thermogravimetric analysis (TGA), scanning and transmission electron microscopy (TEM, SEM), atomic force microscopy (AFM). The results obtained provide evidence of intercalation of salt molecules within the clay layers, as well as good interaction with the polymer, showing the presence of intercalated and exfoliated structures. The nanocomposites show better thermal stability compared to virgin polyamide-6, which is examined by thermogravimetric analysis (TGA). An evaluation of the mechanical properties of the nanocomposites is carried out as a function of clay loading and PA6 matrix type. The Young's modulus and yield strength are measured in order to define the mechanical behaviour. PA6 filled with 5% Maghnite has better mechanical performance; this is due to the dispersed state of the Mag-CTA in the PA6 matrix. The improvement of the efficiency of the process adequate to the retention of the maximum of toxic elements and the effects of the initial pH of a solution and the contact time on the adsorption efficiency are studied.

Keywords: Interlayer distance, In situ polymerization, Maghnite, Matrix, Polyamide-6, Thermogravimetric analysis (TGA)

Polymeric layered silicate nanocomposites have been a new class of materials for some decades. The properties of these materials have developed considerably compared to those of virgin polymers. They have more important characteristics than conventional materials due to the strong interaction between the material components and can be synthesized by a simple and inexpensive process¹⁻³. Polymer/clay nanocomposite has been used in various types of consumer products such as barrier layer materials, beverage packaging, protective coatings, bottle applications and adhesive molding components⁴⁻⁶. Since the early 1990s, a new class of composites involving nanoscale lamellar clay particles has emerged as filler. This takes us from a micrometer size with traditional fillers to a nanometer scale with clays, hence the concept of nanocomposites

or polymer-layered silicate nanocomposites. The improved properties include increased modulus, fire resistance and impermeability of these materials^{7,8}. Clay mineral reinforcing materials is widely used in the improvement of many polymer properties, such as thermal properties, mechanical properties, gas barrier, flame retardancy, debility and many others⁹⁻¹¹. Polyamide-6 (PA6) is an important type of thermoplastic nanocomposite with excellent solvent resistance. Polyamide-6 layered silicate nanocomposites have the advantage of adding biodegradability to traditional nanocomposite properties^{12,13}. They can be prepared by in situ polymerizations by opening a ϵ -caprolactam ring using a conventional initiator to induce polymerization in the presence of organic clay. Giannelis used montmorillonite exchanged with a

surfactant to demonstrate the dispersion of nanoparticles in the PA6 matrix and to evaluate its contribution to improving the thermal power and mechanical properties of the resulting nanocomposites¹⁴. Polyamide-6 (PA6) has a particularly fast crystallization rate, resulting in disadvantages such as high mould shrinkage and dimensional instability. However, it is important to control the crystallization rate and crystallinity, and then to achieve the desired morphology and properties. The aim of our work is to synthesize and determine the structure-property relationships of nanocomposites polymers based on PA6 and Maghnite used as reinforcing clay. Maghnite is a type of clay from Algeria extracted from the Maghnita deposit in Telemcene, one of the most important smectic montmorillonite clays, with an exchange capacity of 101 meq/100 g. The proportion of $\text{SiO}_2/\text{Al}_2\text{O}_3$ is higher than in other clays worldwide¹⁵⁻¹⁷. Indeed, after chemical treatments, maghnite showed an interesting catalytic capacity in the polymerization of various monomers such as furfuryl alcohol¹⁸ β -pinene¹⁹ and siloxanes²⁰. Firstly, we look at the structural characteristics of three different types of clays: raw clay, soda treated clay and organophilic clay treated with cetyl trimethylammonium bromide or Mag-CTA. The particularity is the simple use of clay from our own region, which is a low-cost solution and has excellent properties. The result of this preliminary work was the selection of the best type of clay for the production of PA6-based nanocomposites. The second section deals with the synthesis of PA6/Mag-CTA nanocomposite, elaborated by in situ polymerization, where Mag-CTA is used both as reinforcement and a catalyst. Several compositions were carried out to evaluate the effects of Mag-CTA content in terms of dispersion quality. The chemical structure was determined using IR analysis. Morphology was studied by SEM, AFM to verify the homogeneity of the PA6/ Mag-CTA systems and the suitability of the dispersion process employed. In addition, XRD, TEM was used to determine whether the degree of exfoliation or intercalation of Maghnite platelets in PA6 was achieved. Thermal and mechanical properties were conducted to assess the thermal stability and mechanical strength of the filled components in comparison to the blank components. The use of polyamide-6/organic clay nanocomposites as an effective adsorbent has been widely studied under different adsorption parameters.

Experimental Section

Materials

ϵ -Caprolactam (grade 99%) and Cetyl trimethylammonium bromide (98%), were commercialized by Sigma-Aldrich Corporation Algeria and used in this work without further purification. The raw Maghnite was acquired from the Algerian Company of Bentonite (BENTAL), with no prior treatment. First, the maghnite was dried in a hot air oven at 100°C for 24 h to remove the moisture content.

Preparation process for Maghnite sodium (Mag-Na) and Maghnite cetyltrimethylammonium (Mag-CTA)

After removing the coarse material through sedimentation, the cleaned raw Maghnite was brought into contact with a 1N sodium chloride solution (20 g of clay in 110 mL) under stirring for 6 h. We then recover the treated Maghnite by siphoning, bearing in mind that the montmorillonite crosses a distance of 10cm every 5 h. It was then rinsed with distilled water in several times, covered with a sintered glass with a porosity equal to 5 (the maximum diameter of the pores is 16-40 μm), then dried in an oven at 110°C, sprayed with a mortar and finally stored in a desiccators²¹⁻²³. The process of converting Maghnite-Na to Mag-CTA lies in the substitution of the existing Na^+ ions on the surface of the montmorillonite layers with alkylammonium cations. The modification of Maghnite-Na to Mag-CTA corresponds to the substitution of Na^+ ions present on the surface of the montmorillonite layers by alkylammonium ions. 25 mmol of CTAB ($\text{C}_{16}\text{H}_{33}\text{N}(\text{CH}_3)_3\text{Br}$), 5 ml of hydrochloric acid and 200 mL of water at 82°C are poured into a beaker, 10 g of Maghnite- Na^+ was then incorporated. After filtration, the Maghnite was washed several times with water to remove the sodium bromide that was formed. At the end of the rinsing process, the Mag-CTA was dried at 120°C, crushed and stored in a desiccators^{24,25}.

Preparation of the nanocomposites

The PA6/ Mag-CTA nanocomposites were obtained by in situ polymerization of ϵ -caprolactam catalyzed by Mag-CTA. In a flask immersed in a bath thermostatically controlled at 120°C, different quantities of Mag-CTA (1,3,5 and 7%) were kept under vacuum before the introduction of 11.3 g of ϵ -caprolactam, the mixture was heated to 125°C for 30 minutes and then the temperature was raised to 250°C for 48 h under magnetic agitation. the

temperature and time of the reaction have been optimized in order to obtain high enough molecular weights and yields. After cooling, the product was ground mechanically. The fine particles were washed in water at 80°C for 1 h²⁶, the PA6/clay nanocomposites were named PA6NC1, PA6NC 3, PA6NC 5 and PA6NC7 according to their clay content (Table 1). In order to better control the reaction of the Nylon 6 nanocomposites, the yield of each component was determined. Table 1 shows the yields achieved with different clay contents (1, 3, 5 and 7%) during the development of the Nylon 6/Mag-CTA nanocomposites. An improvement in the yield of the reaction is observed when the amount of Maghnite-CTA is increased. The cationic nature of the polymerization reaction and the number of active initiator sites in the polymerization reaction are proportional to the amount of maghnite added.

Characterization

The Fourier Transform Infrared (FTIR) spectra were registered on an ATIMATTSON type FTIR Spectrometer in the range 400 to 4000 cm⁻¹. The DRX spectra were performed using a Bruker AXS D8 Advance diffractometer equipped with a LynxEye linear detector Bruker, with a Co radiation K α 1 ($\lambda = 1.540\text{\AA}$) and a scanning range 2 θ from 0 to 70° and a scanning speed of 0.02°/s, at room temperature. The morphology of the organophilic maghnite specimens and that of the nanocomposites were evaluated by a TEM meter, Philips CM 120, under an accelerating voltage of 120 kV. Scanning electron microscope photographs of the cracked surface of the tensile specimens were taken using the JEOL JEM-5800 with an accelerating voltage of 20 kV. A topographical study of the surfaces usually gives information on the growth of thin layers and especially oxide layers. A calibration of the near-field microscope "JSPM-4200" can be performed in contact mode or in tapping mode, depending on the standard called reference standard or metal grid, and thanks to the magneto-optical Kerr effect. It should be remembered that resolution is often problematic in atomic force microscopy (AFM), due to the size of

the probe. The thermal stability of the materials was measured with a Shimadzu TGA 51, using an air flow rate of 50 ml/min and a heating rate of 10.0 °C/min. The weight of each sample used was 5.0 ± 0.5 mg. All mechanical tests were performed on a LLOYD LR/10KN Universal tensile tester at 25°C. The test specimens used to measure the strength and stiffness of the nanocomposites were made using a specific punching device, corresponding to the NF EN ISO 527-2 standard, according to the principle of category 1A specimens. Uni-axial tensile tests were carried out at an average rate of 60 mm.min⁻¹ until the specimens broke.

Results and Discussion

FTIR Analysis

Examining the spectrum of Maghnite-CTA (Mag-CTA-(OCEC)) according to Fig. 1(a), the 400-3700 cm⁻¹ region of the Maghnite spectrum shows characteristic bands for O-H, Si-O as well as Al-O, Al-OH, Al-Fe-OH, Al-Mg-OH vibrations. Bands at 3619 and 916 cm⁻¹ are observed which are typical of dioctahedral maghnite, bands corresponding to AL-AL-OH bending vibrations are observed at 914 cm⁻¹. There are also bands at 628 cm⁻¹ attributed to Si-O-Al

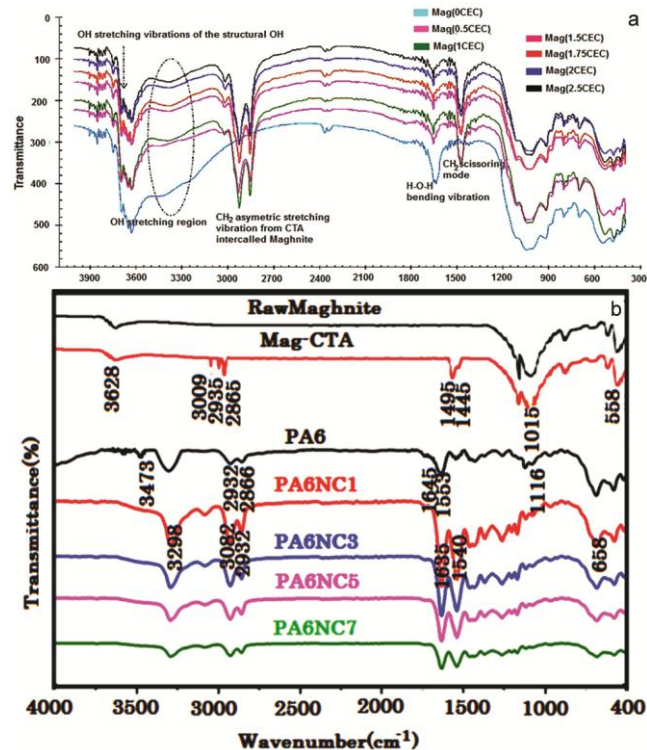


Fig. 1 — (a) FTIR spectra of several clays analyzed Mag-(0.5-1.5-1.75-2-2.5) (CEC); (b) FTIR spectrum of virgin PA6, Mag-CTA and PA6NC.

Table 1 — Experimental conditions for the preparation of Nylon 6/Mag-CTA nanocomposites

Organo-clays	Nylon 6	Time (h)	Yields (%)
PEDOT/Mag-CTA1	11.3	48h	79.2
PEDOT /Mag-CTA3	11.3	48h	85.1
PEDOT /Mag-CTA5	11.3	48h	95.3
PEDOT /Mag-CTA7	11.3	48h	96.1

bonds, and bands at 3435 and 1641 cm^{-1} correspond to the OH deformation frequencies of trapped water molecules. The Si-O out-of-plane stretching band occurs in Maghnite (Mag-CTA-(OCEC)) at 1091 cm^{-1} . Figure 1 shows the intensity and amount of adsorbed water for all analyzed clay samples. The adsorbed water contributes to the H-O-H bending region (1650-1700 cm^{-1}) and the O-H stretching region (3229-3487 cm^{-1}). This band is progressively shifted with increasing surfactant concentration from 1629 cm^{-1} and 1633 cm^{-1} (for Maghnite (Mag-CTA-(OCEC)) and (Mag-CTA-((0.5CEC)) sample, respectively) and to 1639 cm^{-1} (for (Mag-(2.5CEC)) sample). At the same time, the intensity of this absorption decreases significantly. We see a decrease in the intensity of the band that reflects the larger amount of hydrogen-bonded H_2O molecules that are present in organophilic clays. This phenomenon can be explained by the lower H_2O content resulting from the replacement of hydrated cations by CTAB⁺ ions. With the intercalation of the surfactant, the surface characteristics of the clays are changed, i.e. the hydrophilic surface of the maghnite fraction has become hydrophobic. H_2O -containing molecules clustered around exchangeable cations are polarized due to their proximity to the exchangeable cation, with the oxygen of the H_2O remaining oriented towards the metal cation. The intercalation of CTAB is expected to increase such polarization. The FTIR spectra of the Mag-CTA-(0.5-1-1.5-1.75-2-2.5) CEC composites are in the range of 2800-3000 cm^{-1} . The intensities of the two strong adsorption bands at 2922 and 2852 cm^{-1} correspond to the antisymmetric and symmetric CH_2 stretching modes of the amine, respectively, and increase progressively with the stacking density of ammonium chains in the maghnite galleries. Simultaneously, symmetric and antisymmetric C-H stretching of the $-\text{CH}_3$ end groups appears at 2868 and 2956 cm^{-1} , respectively, and depends on the packing density of the amine chains. This means that the intensity of the absorption bands is largely dependent on the stacking density of the amine chains in the maghnite galleries. The change in the wave number of the antisymmetric CH_2 stretching absorption band represents only a slight shift of 8 cm^{-1} from 2924 cm^{-1} for Mag-CTA-(0.5CEC) to 2920 cm^{-1} for Mag-CTA-(2.5CEC). Narrow absorption bands that appear around 2920 ($\nu_{\text{as}}(\text{CH}_2)$) and 2852 cm^{-1} ($\nu_{\text{as}}(\text{CH}_2)$). Following the intercalation of CTAB into maghnite, new infrared adsorption bands appear between 1480 and 1419 cm^{-1} . (Ref. 27)

The IR spectra of raw maghnite, Mag-CTA, pure PA6 and various nanocomposites obtained are shown in Fig. 1(b). The IR spectra of raw maghnite and Mag-CTA reveal that maghnite is a clay mainly composed of montmorillonite. The IR spectrum of Mag-CTA shows characteristics which result from the combination of the specific groups of the montmorillonite and the CTAB molecule. The FTIR spectra of PA6 and PA6NC are shown in Fig. 1b. As shown in Table 2, the characteristic bands of N-H, C-H, C-H, C-H, C-O, amide I, amide II and amide V are found. For PA6NC, it is noted that the contribution of the PA6 characteristic bands is much higher than that of montmorillonite. Also, the absorptions of the N-H bond and the C=O bond of amide I, which appear respectively at 3298 and 1635 cm^{-1} , show obvious displacements at frequencies lower than those of pure PA6. Given the abundance of silanol groups on the surface of nanosilica, these results should indicate the existence of hydrogen bonds between PA6NC and nanosilica²⁸⁻³⁰ and high attenuation of the absorption bands relative to the OH groups of water molecules (at 3400 cm^{-1}) indicating the replacement of water molecules with CTA³¹⁻³³.

X-ray Diffraction analysis

Figure 2(a) of the XRD diffractograms of the Maghnite treated with NaCl (Mag- Na^+) resulted in the peak characteristic of the plane (001) of the Mag at $2\theta = 5.5^\circ$, resulting in a layer spacing of 12.89 Å. The XRD performed according to Fig. 2(a) indicate an insertion of the alkyl chains of the "CTAB" surfactant in the Maghnite galleries. As a result of the cationic modification of sodium ions by the cationic surfactant CTAB⁺, an expansion of the maghnite layers takes place. This expansion is measured directly by X-ray

Table 2 — Band assignments of FTIR spectra of PA6 and PA6NC nanocomposites

Functional groups	PA6 Frequency (cm^{-1})	PA6NC Frequency (cm^{-1})
Amide I	1648	1635
Amide II	1553	1540
Amide V		685
Asymmetric elongation C-H	2932	2932
symmetric elongation C-H	2866	2859
Elongation N-H	3473	3082
Shear deformation $-\text{CH}_2$	1433	
Elongation C-C	1116	
Vibration N-H primary amine		3298

diffraction from the basal spacing powder. Fig. 2(a) shows the XDR diagrams of organic CTAB maghnite at various surfactant concentrations and the variation of the d-spacing as a function of the amount of salt in contact with the maghnite. The results obtained indicate that the basal spacing of the smectite fraction increased as expected, depending on the surfactant concentrations. Indeed, for a concentration rate corresponding to 0.5 CEC, indeed, for a concentration rate corresponding to 0.5 CEC, there is a shift of the montmorillonite peak in the (001) plane towards smaller angles $2\theta = 3.0^\circ$ the spacing of Na^+ -Mag would have increased from 12.27 Å to 17.25 Å for Mag-CTA. Nevertheless, for a concentration Mag-CTA rate corresponding to 2.5 CEC, the analysis performed on the modified Maghnite (Mag-CTA) revealed two peaks at $2\theta = 4.5^\circ$ and 2.3° at a frequency of 19.7 Å and 37.918 Å, respectively. The peak intensities are higher in the (001) plane due to a narrower distribution of interlamellar spacing resulting from the presence of CTA ions in the clay sheets, for a concentration level corresponding to 2CEC, Based on the results obtained, the detection of two signals instead of one in the Mag-CTA could be related to the diffraction of planes other than the d_{001} , indicating a high regularity of the modification of the Maghnite. The angle (α) between the alkyl chain and the basal surface is calculated taking into account the length of the CTAB⁺ molecule and the thickness of the envisaged TOT layer. The interfoliar distances of the different samples of Nylon 6/ Mag-CTA processed nanocomposites were obtained from the position of the X-ray diffraction peak [001].

Figure 2b shows the XRD analysis of the different nanocomposites prepared (1, 3, 5 and 7 wt %). The strong clay diffraction peak (Mag-CTA) is not observed on the PA6NC1, PA6NC3 and PA6NC5 units, suggesting that the clays are relatively well exfoliated in the low-filler PA6 matrix. The XRD diffractograms of the PA6NC7 and PA6NC10 nanocomposites show an increase in the value of the d_{001} diffraction peak at $2\theta = 2.80$ and 3.01° respectively, and these XRD diffraction spectra display spacings of 31.52 and 29.32 Å. As a result of previous work described in the literature, We report hereafter that The PA6 matrix can take two different crystallographic forms: the pseudo-hexagonal form γ and the monoclinic form α , for the monoclinic form, hydrogen bonds are formed between antiparallel chains, contrary to the pseudo-hexagonal form, hydrogen bonds are formed between parallel chains,

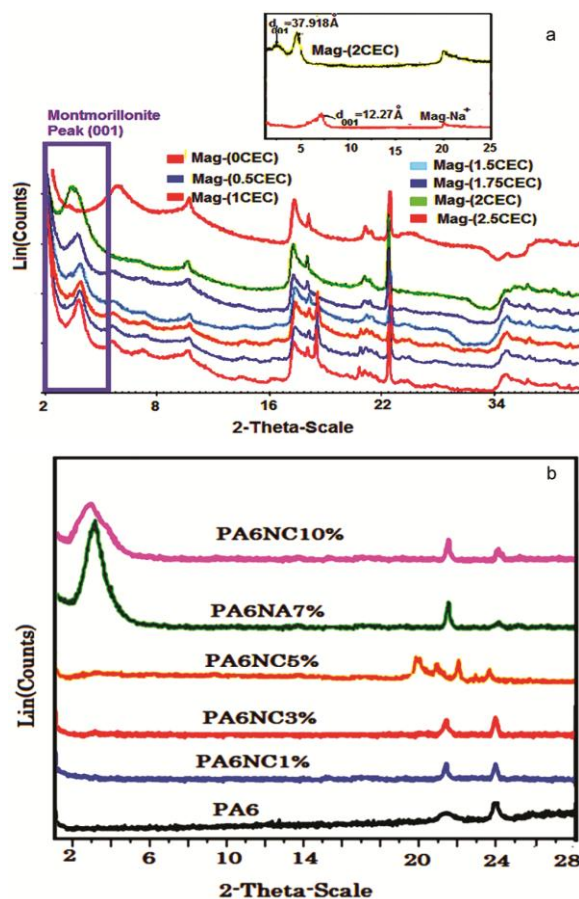


Fig. 2— (a) The XDR patterns of Maghnite and surfactant intercalated Mag-CTA clays; (b) X-ray diffractograms of pure Nylon 6 and Nylon 6/Maghnite-CTA nanocomposites.

this causes the twisting of the molecular chains in zigzag planes. The form α is identified in DRX diffractograms by the peak located approximately at $2\theta = 24^\circ$ ($d_{001} = 3.70 \text{ \AA}$), in addition, the peak that characterizes the crystalline form γ appears at approximately $2\theta = 21.5^\circ$ ($d_{001} = 4.12 \text{ \AA}$). The introduction of the treated clay varied the shape and intensity of these peaks by modifying the crystallinity of the PA6 matrix. While increasing the clay content increases the intensity of the peak characterizing the γ -crystalline form, the addition of clay favored the formation of the γ -form, which follows a heterogeneous nucleation mechanism, and similar results were previously obtained by Jiang *et al.*³⁴⁻³⁶.

Transmission Electron Microscopy analysis

The X-ray diffraction technique allowed us to specify the dispersion mode of the organophilic Maghnite in the PA6 matrix (intercalated, exfoliated) and in order to consolidate these results, we used transmission electronic microscopy. Figure 3 shows

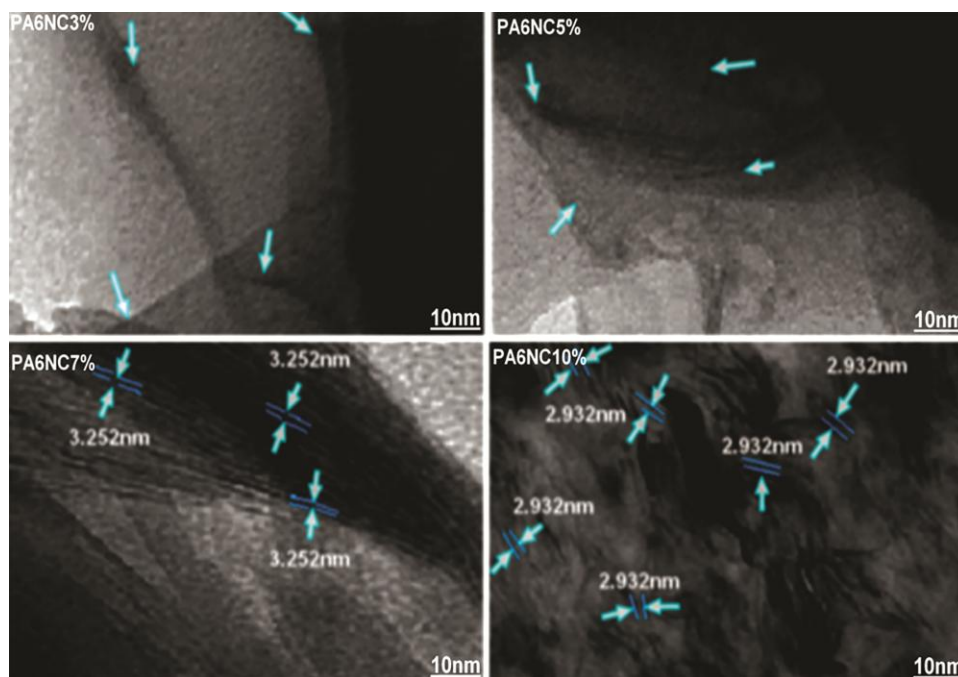


Fig. 3 — TEM micrograph nanocomposites of PA6NC3% (Exfoliated), PA6NC5% (Exfoliated) and PA6NC7%(Intercalated), PA6NC10% (Not miscible).

the TEM images of the synthesized nanocomposites. The clay layers are shown in the images as lines. The individual lines correspond to an exfoliated structure and the ordered lines to an intercalated structure. Figure 3 shows the TEM images of Mag-CTA and the different PA6CN % nanocomposites processed. The TEM image of the PA6NC3 and PA6NC5 nanocomposites for low clay contents shows an exfoliated morphology, and the micrographs of the PA6NC7 nanocomposites are in favor of an intercalated morphology where the order of the clay particles is maintained. Figure 3 of the PA6NC3, PA6NC5 nanocomposites shows some disorder in the morphology of the clay. The somber lines correspond to the monolayer silicates. The clay plates are separated which results in an exfoliated structure. However, nanocomposites made with 10% clay are immiscible, large groups are clearly observable and the existence of intercalated clay regions or total exfoliation is probably due to the limited diffusion of PA6 in the organophilic clay layers. The morphological description obtained by TEM largely corroborates the X-ray diffraction results.

Scanning Electron Microscopy Analysis

Figure 4 presents the SEM images of several PA6/organoclay nanocomposites produced. The images of the nanocomposites reveal diverse morphologies with various sizes and the type of modified organic clay has a very significant impact on

its dispersion in the PA6 polymer matrix. The nanocomposites from Mag-CTA showed a partial degree of dispersion mainly due to the presence of nanoscale PA6 particles (spherical shaped particles) and clay sheets. However, the manufactured nanocomposites have porous and homogeneous particles, whose morphology varies according to the percentage of clay used. The heterogeneity of the shape is due to the heterogeneous dispersion of the PA6 within the organo-modified clay galleries.

Atomic Force Microscopy analysis

The 3D topographic image in Fig. 5 reflects a lamellar structure in the form of lamellar stacks, which are separated from each other by regions without a particular structure that constitutes the amorphous interfibrillar region. Figure 5 also shows that the clay layers of the PA6NC nanocomposites are smooth with low roughness, and that the grain size decreases significantly for the PA6NC1, PA6NC3 nanocomposites, indicating that the clay has a significant effect on the surface morphology. However, Figure 5 shows that the PA6NC10 nanocomposites formed in the deep part of the film are most often agglomerations.

Thermogravimetric analysis

Thermogravimetric analysis (TG) of maghnite and all Maghnite-CTA studies samples are shown in

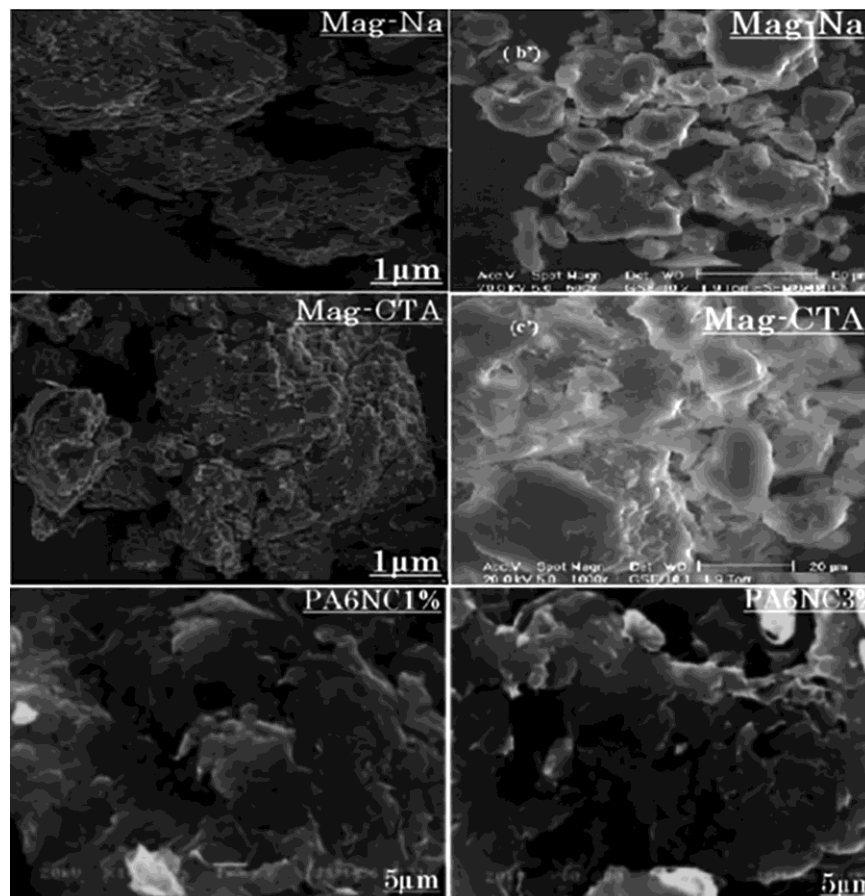


Fig. 4 — SEM images of: Mag- Na^+ , Mag-CTA, PA6NC1%, PA6NC3%

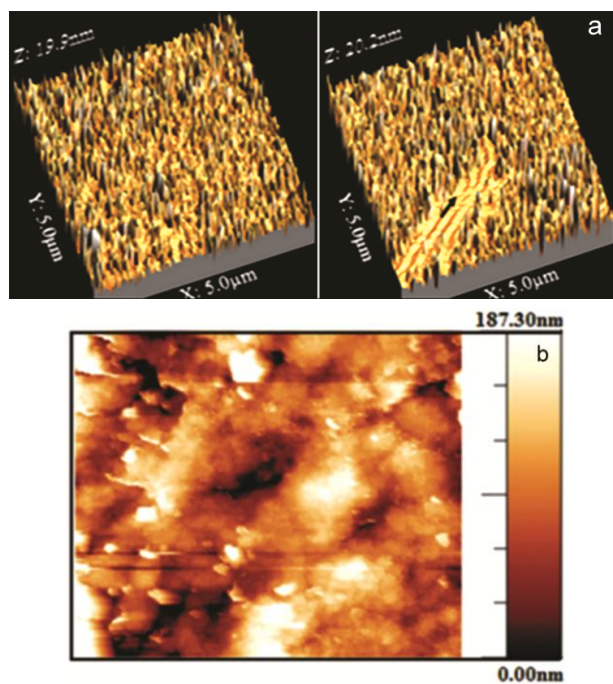


Fig. 5 — (a) 3D image shows the topography PA6NC1% and PA6NC 3%; (b) Morphology of PA6NC10%

Fig. 6(a). Different stages of mass loss are identified. The decomposition of CTAB took place in two stages. The first stage is observed at a temperature below 200°C , at exactly 50.78°C for Mag-CTA-(0CEC) and 23.0°C for Mag-CTA(2.5CEC) with a mass loss ranging from 7.02 to 1.36% respectively. It is due to the loss of mass caused by the dehydration of physically adsorbed water and water molecules around metal cations such as Na^+ and Ca^{2+} on the exchangeable sites of maghnite. Only minimal dehydration is observed for (Mag-CTA-(0.5-1-1.5-1.75-2-2.5) CEC) and it decreases with increasing organophilicity. This probably corresponds to interlayer water trapped by the CTAB ammonium salt. The second stage is between 200 and 400°C . This second loss of mass is attributed to the decomposition of the CTAB surfactant by the departure of long-chain alkyl groups. The ATG results of these organoclays indicate that the phenomenon is specific to alkyl cation groups binding to external surfaces and easily accessible ends. When the surfactant concentration is particularly low, organic cations exchange with Na^+

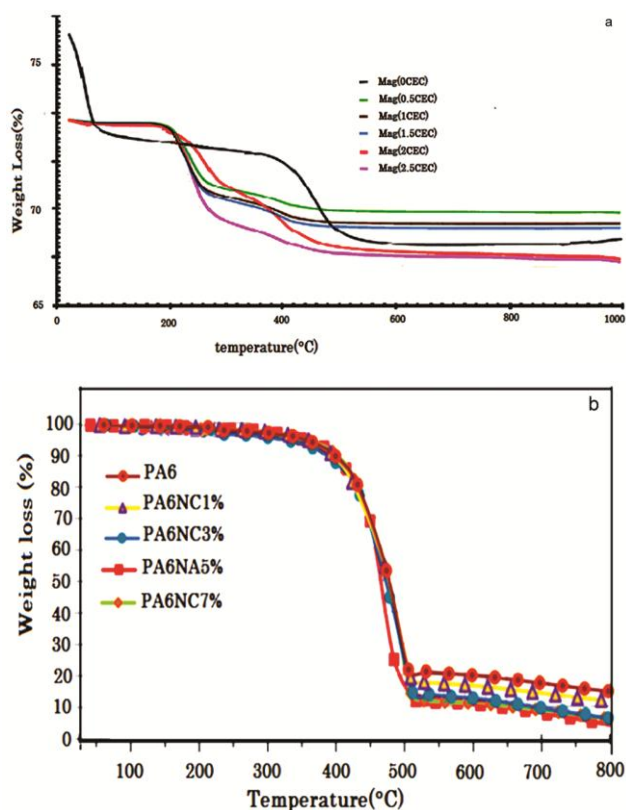


Fig. 6 — (a) TG results of raw Maghnite, and organoclays Mag-CTA; (b) TG curves of pure PA6 and different PA6NC nanocomposites.

ions and binds to surface sites mainly through electrostatic interactions. CTAB is supposed to decompose or burn at 205°C, so the third peak that appeared was very close to this critical temperature. The third step manifested by the loss of mass above 400°C was attributed to the loss of dehydroxylation of the structural OH units of the maghnite. This is shown in Fig. 6(a) at 461.3 °C for maghnite and varied from 411 to 492°C for Mag-CTA (0.5CEC) and Mag-CTA (2.5CEC), respectively. These peaks are, as before, assigned to the dehydroxylation of the maghnite. It is observed that there is a considerable shift towards lower temperatures in the dehydroxylation of organoclays³⁷.

Thermogravimetric analysis (TGA) of the samples was performed under a nitrogen atmosphere between room temperature and 800°C. Results are presented in Fig. 6(b). Results clearly show the improvement in the thermal stability of polyamide-6 when incorporating wt % by weight of organoclays. The temperatures associated with a 20% loss in initial mass of the T₂₀ composites analyzed increase by 6 to 22°C compared to the raw polyamide-6. Also for T₅₀,

degradation temperatures of 50% of the initial mass, which are improved from 12 to 25°C. The improvement in the thermal behavior of polymer-clay nanocomposites compared to raw polymers can be explained on the one hand, by the formation of charbon (from clay) which serves as a barrier between the mass transport and as isolator between the polymer and the surface zone where the polymer breaks down and on the other hand, by restricting the thermal dissociation of the polymer portions located in the clay galleries. Indeed, T₂₀ and T₅₀ are almost identical in both cases. The inclusion of only wt % modified clay improves the degradation temperatures T₂₀ and T₅₀ respectively compared to polyamide-6. Beyond a concentration of 5wt%, there is little difference between the degradation profiles suggesting a threshold effect³⁸. Above a concentration of 5%, there is little difference between the degradation profiles suggesting a threshold effect. These results indicate that the introduction of clay can change the decomposition mechanism of Nylon 6 at high temperatures (240 to 500°C) furthermore, the thermal stability of the prepared nanocomposites is related not only to the clay content but also, to the state of the clay in the polymer matrix, to the surface between the polymer matrix and the clay.

Mechanical properties

This section contains a comparison between the mechanical properties of the pure polymer and the nanocomposites produced. The impact of the modified clay on the tensile strengths of the PA6 is illustrated in Fig. 7. This figure shows the positive evolution of the "PA6/ Mag-CTA " nanocomposite curve. The addition of modified clay increases the polymer's rigidity and tensile strengths. This can be explained by the effect of clay particles on the size of the PA6. These spaces absorb impact energy and limit the propagation of cracks. This indicates that the reinforcement of the polyamide-6 by the modified clay gives it greater strength. The greatest improvement in tensile strengths is obtained for compositions below 3wt%. This growth is explained in particular by better adhesion between the filler and the matrix and by the good dispersion of the filler in the polyamide-6 matrix. Figure 7 presents an improvement in the Young's modulus of nanocomposites compared to pure PA6. The stiffness of nanocomposites visibly increases with increasing filler content. This increase is caused principally through improved interfacial polystyrene/clay

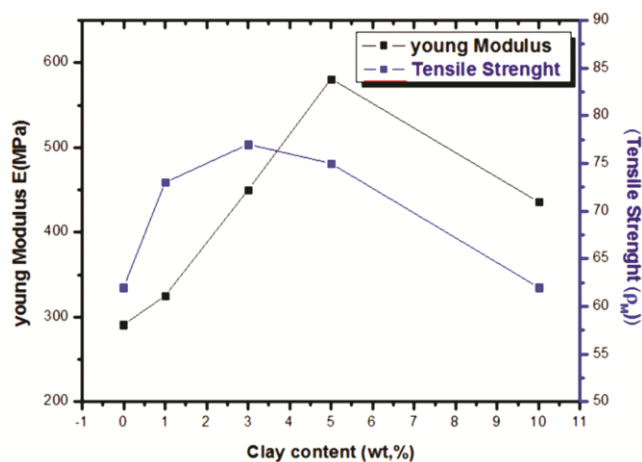


Fig. 7 — Evolution of the Young modulus and tensile strength, as a function of the clay content.

adhesion due to good dispersion of the clay filler in the polystyrene matrix. Experimental results showed an optimal mass ratio (5wt% Mag-CTA). It is attributed to the creation of parasitic connections between the Mag-CTA and the ends of the polymer chains. This results in uniformity and rigidity of structures. The number of connections increases with the presence of the Mag-CTA-wt%^{39,40}. The Young's modulus increases more strongly for exfoliated nanocomposites. Nanocomposites showed greater improvements in Young's modulus, the loads make the polymer more resistant to the tensile force small, well-dispersed particles generally increase the tensile strength properties, which is the case with clay.^{41,42}

Adsorption of heavy metals by raw clays, organoclays and prepared nanocomposites

In order to determine the influence of pH on the adsorption of Co (II), Cu (II), Cd (II) and Ni(II) on clays, a series of experiments was carried out using solutions containing these different metals at concentrations of 100 mg/L in contact with raw clays at a concentration of 10g/L and for pH values varying between 1 and 8. We have limited to $\text{pH} \leq 6.71$ for Cd(II), $\text{pH} \leq 6.70$ for Co(II), $\text{pH} \leq 5.65$ for Cu(II) and $\text{pH} \leq 7.6$ for Ni(II) to avoid precipitation of heavy metals. The results obtained are shown in Fig. 8.

The analysis of these results shows that the amount of Cd(II), Co(II), Cu(II) or Ni(II) adsorbed on raw clay increases with increasing pH. When the pH varies between 2 and 6.71, the amount of Cd(II) adsorbed by maghnite varies from 8.23 to 9.03 mg/L; similarly, when the pH varies between 2 and 6.7, the amount of Co(II) adsorbed by maghnite varies from 6.40 to 9.62 mg/L; and when the pH varies between

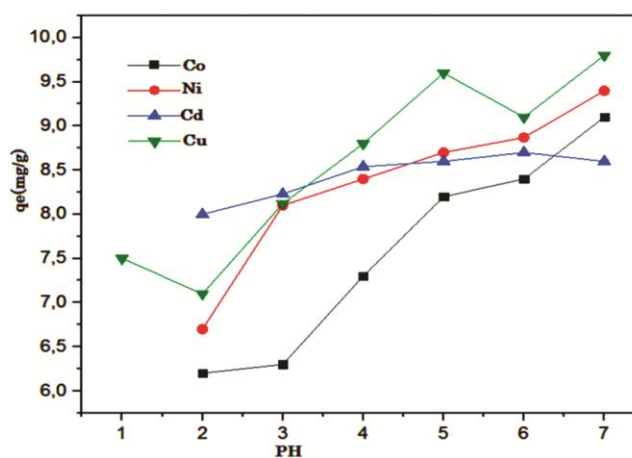


Fig. 8 — Influence of pH on the adsorption of Cd(II), Co(II), Cu(II) and Ni(II) on clay: crude Maghnite; $\text{C0} (\text{M}^{2+}) = 100\text{mg/L}$; Clay concentration = 10g/L and $T=20^\circ\text{C}$.

1.5 and 5.65, the amount of Cu(II) adsorbed on maghnite varies from 7.38 to 9.96 mg/L; and finally, when the pH varies between 1.5 and 7.6, the amount of Ni(II) adsorbed on raw maghnite varies from 6.72 to 9.96 mg/L. At very acidic pH values ($\text{pH} < 1.5$), the removal rate of Cd(II), Co(II), Cu(II) and Ni(II) is greatly reduced. By adding H^+ ions, the pH is decreased to values below 2.5, which neutralises the negative charge of the clays and consequently hinders the adsorption of Cd(II), Co(II), Cu(II) and Ni(II) which are present in the cationic form Cd^{2+} , Co^{2+} , Cu^{2+} , Ni^{2+} in this pH range. When the pH increases ($1 < \text{pH} < 8$), there is a decrease in H^+ cations which favours the adsorption of Cd^{2+} , Co^{2+} , Cu^{2+} and Ni^{2+} , on the negative surface of the clay. The adsorption of Cd^{2+} , Co^{2+} , Cu^{2+} and Ni^{2+} , on the negative surface of the clay (Fig. 9)⁴³⁻⁴⁸.

We observe that the lack of a chelating group on the structure of CTAB and its occupation of negative sites on the surface of clays by quaternary ammoniums are negative sites on the clay surface by quaternary ammoniums are responsible for the low retention of heavy metals. On the other hand, the presence of negative charges on the raw clays leads to a better adsorption compared to the clays modified clays. The nanocomposites have allowed the retention of heavy metals, but retention rates remain lower than for clays, which have a much higher surface load.

Effect of contact time

The thermodynamic equilibrium between the adsorbate in the liquid phase and the adsorbate fixed on the solid is reached with a speed that depends not

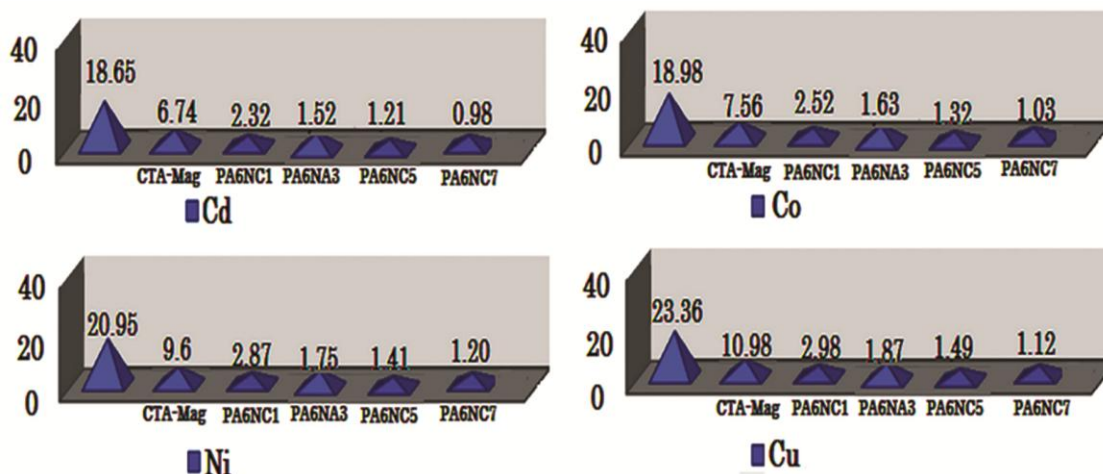


Fig. 9 — Adsorption quantities q_m in mg/g of heavy metals by raw and modified maghnite and modified maghnite(Mag-CTA) and nanocomposite.

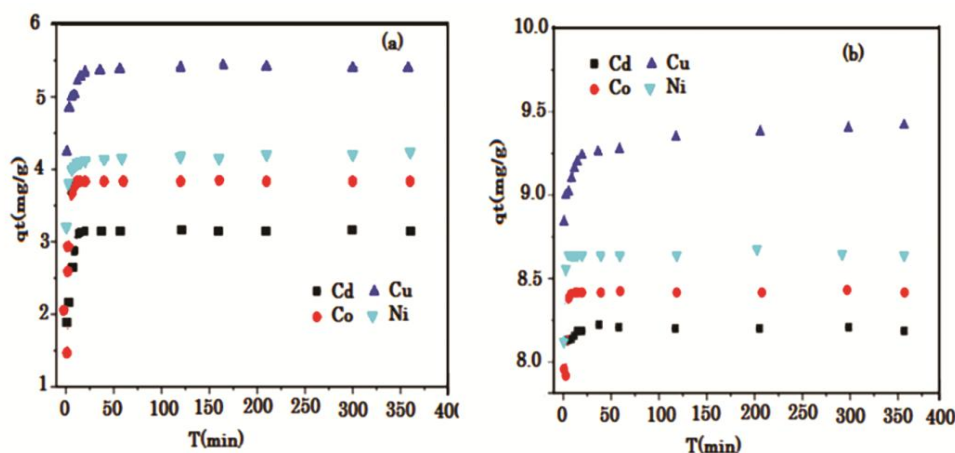


Fig. 10 — Influence of stirring time on the adsorption of Cd(II) at pH 6.67, Co(II) at pH 6.96, Cu(II) at pH 5.5 and Ni(II) at pH 7.5 on clay: (a) Maghnite and (b) Mag-CTAhnite; C_0 (M^{2+}) = 100mg/L; clay concentration = 10g/L

only on the speed with which the solid is reached with a speed that depends not only on the speed with which the constituents diffuse in the adsorbent and in the fluid but also on the interaction adsorbent-adsorbate interaction. The study of the adsorption of a compound on an adsorbent allows us to examine the influence of the contact time on its retention. The fixation of heavy metals is often described as a reaction time dependent process. The results of some work on fixation kinetics range from short times (a few minutes to 4 hours)^{49,50} to times exceeding 24 h. The knowledge of the equilibrium time is necessary to establish the adsorption isotherms. This parameter is studied in the case of the retention of copper and nickel by raw clays and modified clay (Mag-CTA). The shape of the curves shown in Fig. 10 is typical of saturation curves with a slight qualitative

and quantitative difference. Equilibrium is reached more quickly in the case of Co(II) (6 min), Ni(II) (10 min) and Cd(II) (15 min) than in the case of Cu(II) (120 min). Thus, raw maghnite has a higher adsorption capacity for cadmium, cobalt, nickel and copper ($q_e = 8.20$ mg/g; 8.44 mg/g; $q_e = 8.71$ mg/g and 9.48 mg/g respectively) than modified maghnite ($q_e = 3.15$ mg/g; 3.83 mg/g; $q_e = 4.23$ mg/g and 5.41 mg/g respectively). It can be seen that copper has a good affinity for both clays. The Langmuir adsorption isotherm is based on the assumption that the adsorbate molecules form a monolayer on the surface of the adsorbent^{51,52}.

The adsorption energy of all sites is identical and independent of the presence of adsorbed molecules on neighboring sites (homogeneous surface and no interaction between adsorbed molecules). Langmuir's

isotherm is widely used to describe the adsorption reaction and can be represented by equation E1.

$$\frac{C_e}{q_e} = \frac{C_e}{q_m} + \frac{1}{K_L q_m} \quad (\text{E1})$$

Where,

C_e : concentration of the solute at equilibrium (mg/L) q_e : quantity adsorbed at equilibrium (mg/g)

q_m : maximum quantity adsorbed at saturation of the monolayer or maximum adsorption capacity (mg/g) K_L : equilibrium adsorption constant, temperature dependent (L/g) The adsorption capacity of the Langmuir monolayer (q_m) gives the amount of metal required to occupy all available sites per unit mass of the sample.

All the R^2 correlation coefficients exceed 0.89, which shows that the experimental results coincide perfectly with the linear form of the Langmuir model. Results coincide perfectly with the linear form of the Langmuir model. According to Table 1, we can see that the adsorption capacity q_m of Maghnite at 25°C is two and a half times higher than that of Mag-CTA. The highest adsorption capacity is observed for copper because of its small size compared to the others and so on. The adsorption of cadmium, cobalt, copper and nickel by Mag-CTA and crude maghnite is dominated by the cation exchange phenomenon. This phenomenon of cation retention appears with a preferential order of selectivity: $\text{Cu}^{2+} > \text{Ni}^{2+} > \text{Co}^{2+} > \text{Cd}^{2+}$

Conclusion

The results show that PA6/ Mag-CTA nanocomposites have better thermal stability and higher Young's modulus, impact strength and tensile strength than PA6. However, when the organic clay content reaches 5 wt%, the thermal stability, Young's modulus, impact strength and tensile strength decrease. Characterization of the structure and thermal behavior of these materials has highlighted the effect of the structural conception of surfactant substances on the morphology and thermal degradation and mechanical properties of nanocomposites. Exfoliated nanocomposites offer greater thermal stability than virgin polyamide-6 and could potentially serve as flame retardant materials. Exfoliated composites with a loading rate of 5wt% show better results in terms of thermal and mechanical properties. The pH-dependent study of the adsorption showed that the amount of cobalt (II),

cadmium (II), copper (II) and nickel (II) adsorbed on the two raw clays and the modified clay increases with increasing pH. For very acidic pH values, the removal of the four heavy metals is very low. The best retention of heavy metals is given by modified clays. The lack of a chelating group on the CTAB structure and its occupation of the negative sites on the surface of the clays are responsible for the low retention of heavy metals compared to raw clays and nanocomposites. The structure of the polymers allowed the chelation of heavy metals, but the number of chelated metals was lower than the number of complexed metals on the basal surface of the raw clays, which caused the low retention of heavy metals by the nanocomposites compared to the raw clays.

Reference

- Mrah L, *Polym Polym Compos*, 30 (2022) 09673911221080302.
- Chabane M, Melkaoui C, Dahmani B, Boudjenane Z & *Annales de Chimie - Science des Matériaux*, 45 (2021) 191.
- Bashal A H, Khalafalla M & Abdel-Basset T A, *Arab J Sci Eng*, 46 (2021) 5859.
- Megherbi R, Mrah L & Marref M, *Iran Polym J*, 31 (2022) 223.
- Rathore B S, Chauhan N P S, Rawal M K, Rawal M K, Ameta S C & Ameta R, *Polym Bull*, 77 (2020) 4833.
- Ferreira W H, Silva C A & Andrade C T, *Polym*, 201 (2020) 122625.
- Tibayan E B, Muflikhun M A, Villagracia A R C, Kumar V & Santos G N C, *J Mater Res Technol*, 9 (2020) 4806.
- Mohammadlou M, Maghsoudi H & Jafarizadeh-Malmiri H, *Int Food Res J*, 23 (2016) 446.
- Wang Y, Hou D -F, Ke K, Huang Y-H, Yan Y, Yang W & Yang M-B, *Polym*, 212 (2021) 123173.
- Zhu T T, Zhou C H, Kabwe F B, Wu Q Q, Li C S & Zhang J R, *Appl Clay Sci*, 169 (2019) 48.
- Cazotti J C, Salvato R C, Alves G M & Moreira J C, *Polym Bull*, 76 (2019) 6305.
- Thakur V, Gohs U, Wagenknecht U & Heinrich G, *Macromol Chem Phys*, 213 (2012) 729.
- Khiati Z, Mrah L, *J Chem Technol*, 29(2) (2022) 117.
- Liu L, Jiang Y, Zhao H, Chen J, Cheng J, Yang K & Li Y, *ACS Catal*, 6 (2016) 1097.
- Alhazime A A, El-Shamy Nesreen T, Benthani Kaoutar, Barakat Mai M E & Nouh Samir A, *J Polym Eng*, 41 (2021) 119.
- Roghani-Mamaqani H, Haddadi-Asl V, Khezri K & Salami-Kalajahi M, *J Polym Res*, 21 (2014) 333.
- Jeon I Y, Choi H J, Jung S M, Seo J M, Kim M J & Dai L, *J Am Chem Soc*, 135 (2013) 1386.
- Pareek Vikram, Bhargava Arbit, Gupta Rinki, Jain Navin & Panwar Jitendra, *Adv Sci Eng Med*, 9 (2017) 527.
- Gee R P, *Colloids Surf A: Physicochem Eng Asp*, 481 (2015) 297.
- Bujňáková Z, Baláz M, Dutková E, Baláz P, Kello M, Mojžišová G, Mojžiš J, Vilková M, Imrich J & Psoška M, *J Colloid Interf Sci*, 486 (2017) 97.
- Abulyazied D E & Ene A, *Polym*, 13 (2021) 4401.

- 22 Zhuo H, Mei Z, Chen H & Chen S, *Polym*, 148 (2018) 119.
- 23 Mahmood K, Hashmi W, Ismail H, Mirza B, Twamley B, Akhter Z, Rozas I & Baker R J, *Polyhedron*, 157 (2019) 326.
- 24 Poonam Y, Shobhana S, Suman K, Seema & Mamta R, *Indian J Chem*, 60A (2021) 1539.
- 25 Lijun R & Chunlan Y, *Indian J Chem*, 57A (2018) 626.
- 26 Garcia-Lopez D, Gobernado-Mitrea I, Fernandezb J F, Merinoa J C & Pastora J M, *Polym*, 46 (2005) 2758.
- 27 Mrah L, Marref M and Megherbi R, *J Polym Engin*, 42 (2021) 57.
- 28 Chang J H, *Rev Adv Mater Sci*, 59 (2020) 1.
- 29 Sangu V, Yamuna T, Anu Preethi G & Sineha A, *Indian J Chem Technol*, 28 (2021) 479.
- 30 Sun Y, Mei J, Hu H, Ying J, Zhou W & Zhao X, *Rev Adv Mater Sci*, 59 (2020) 434.
- 31 Mrah L, Meghabar R, Belbachir M, *J. Nanomed. Nanotechnol* 6 (2015) 1000263.
- 32 Vergnes B, *Polym Process*, 34 (2019) 482.
- 33 Kavitha T, Sarojini P, Soundaranayaki V & Pandiselvam S, *Int J Manag Technol Eng*, 8 (2018) 1915.
- 34 Penel-Pierron L, Depecker C, Séguéla R & Lefebvre J –M, *J Polym Sci Part B: Polym Phys*, 39 (2001) 484.
- 35 Ahmad M B, Gharayebi Y, Salit M, Hussein M & Kamyar Shamel, *Int J Mol Sci*, 12 (2011) 6040.
- 36 Saadatfar M & Soleimani A, *Adv Mater Res*, 403 (2011) 1188.
- 37 Kolesov I, Androsch R & Mileva D, *Colloid Polym Sci*, 291 (2013) 2541.
- 38 Abhijit P, Sarat Chandra K, Partha M, Shubhamoy C & Rajarshi G, *Indian J Chem*, 56A (2017) 1317.
- 39 Abolghasemi Fakhri L, Ghanbarzadeh B, Dehghannya J, Abbasi F & Ranjbar H, *Food Packag Shelf Life*, 17 (2018) 11.
- 40 Cao K, Guo Y, Zhang M, Arrington C B, Long T E, Odle R R & Liu G, *Macromol*, 52 (2019) 7361.
- 41 Kajaks J, Kalnins K, Uzulis S & Matvejs J, *Cent Eur J Eng*, 4 (2014) 385.
- 42 Goodarzi V, Jafari S H, Khonakdar H A & Ghalei B, *J Membr Sci*, 445 (2013) 76.
- 43 Sen T K & Gomez D, *Desalination*, 267 (2011) 286.
- 44 Abollino O, Giacomino A, Malandrino M & Mentasti E, *Appl Clay Sci*, 38 (2008) 227.
- 45 Akpomie K G, Ezeofor C C & Olikagu C S, *Environ Sci Pollut Res*, 25 (2018) 34711.
- 46 Macro Cinelli, Stuart R Close, Mallikarjuna N Nadagouda, Jerzy Blaszczyński, Roman Slowinski, Rajender S Varma & Kerry Kirwan, *Green Chem*, 17 (2015) 2825.
- 47 Liu J, Dong Z, Ding W, Zhao P, Sun J, Jin X & Li R, *Water Sci Technol*, 66 (2012) 321.
- 48 Moshood Abioye A, Faraji S & Ani F N, *J Technol*, 79 (2017) Please tell me pages number.
- 49 Khan M Z H, Tareq F K, Hossen M A & Roki M N A M, *J Eng Sci Technol*, 13 (2018) 158.
- 50 Guerra D J L, Mello I, Resende R & Silva R, *Water Resour Indust*, 4 (2013) 32.
- 51 Yue T, Han H, Sun W, Hu Y, Chen P & Liu R, *Hydrometallurgy*, 165 (2016) 238.
- 52 Doshi H, Seth C & Ray A, *Curr Microbiol*, 56 (2008) 246.